Chemical and Biological Engineering Publications   Chemical and Biological Engineering

12-26-2012

Thermodynamics of Symmetric Diblock Copolymers Containing Poly(styrene-ran-styrenesulfonic acid)

Nacú B. Hernández
Iowa State University, nacu23@iastate.edu

Calvin Benson
Iowa State University

Eric W. Cochran
Iowa State University, ecochran@iastate.edu

Follow this and additional works at: http://lib.dr.iastate.edu/cbe_pubs

Part of the Polymer Science Commons

The complete bibliographic information for this item can be found at http://lib.dr.iastate.edu/cbe_pubs/37. For information on how to cite this item, please visit http://lib.dr.iastate.edu/howtocite.html.

Thermodynamics of Symmetric Diblock Copolymers Containing Poly(styrene-*ran*-styrenesulfonic acid)

Nacú Hernández, Calvin Benson, and Eric W. Cochran*

Department of Chemical and Biological Engineering, Iowa State University, Ames, Iowa 50011, United States

S *Supporting Information*

ABSTRACT: We examine the thermodynamic behavior of diblock copolymers representing the binary pairs of the ternary system: poly(dimethylsiloxane)/poly(ethylene-*stat*-propylene)/poly(styrene-*ran*-styrenesulfonic acid), $D/E_P/S_S$. We employ small-angle X-ray scattering, electron microscopy, and rheology to characterize the order-to-disorder transition temperature T_{ODT} and lamellar period d of 28 materials with varying molecular weights and sulfonation extents. These data are then interpreted in the context of self-consistent mean-field theory employing the continuous Gaussian chain model to deduce the interaction parameters as a function of temperature and sulfonation extent. We find that while $E_P D$ and $S_S E_P$ are amenable to such treatment, the S_S/D interaction forces $S_S D$ chains to stretch beyond the realm of applicability of the Gaussian chain model.

Poly(dimethylsiloxane-*b*-styrene sulfonic acid)
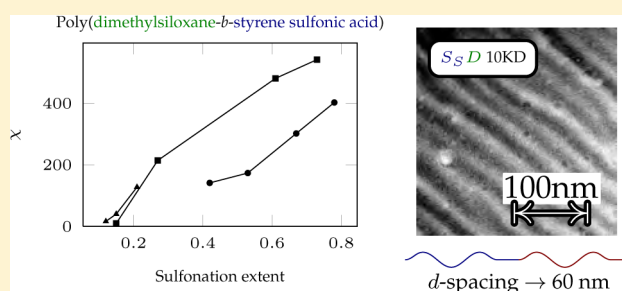
INTRODUCTION

Poly(styrene-*ran*-styrenesulfonic acid) (PS_S) and block copolymers (BCPs) thereof have been studied extensively for applications such as adhesives, water purification membranes,[1,2] and ion exchange membranes for fuel cells.[3,4] Fuel cells have been developed as power sources for a variety of different applications, ranging from consumer electronics to motor vehicles. They are desirable thanks to their high energy efficiency and low emissions. The polymer electrolyte fuel cell (PEFC) has received the most attention for vehicle propulsion because of its high power density.[5] Current research on the PEFC is directed at a number of potential performance improvements: these include new catalysts with enhanced activity and selectivity, membranes permitting operation at higher temperatures which leads to improved catalyst activity, and more effective water management to minimize problems due to membrane dehydration and catalyst flooding.[6,7] Success in these efforts will help alleviate remaining obstacles to economic viability, namely excessive catalyst cost and low power density. Recent work in battery and fuel cell technology has focused on the incorporation of block copolymers (BCPs) containing charged species, e.g., the sulfonic acid (SO_3^-) group, attached as one of the blocks or as part of the main chain giving them the ability to serve as ion exchange materials.[3,4] The use of ionic functional groups modifies the physical and chemical properties of the BCPs by increasing their proton and water transport capabilities, hydrophilicity, melt viscosity, and glass transition temperature (T_g), making them suitable to use in the fuel cell industry as substitutes of the perfluorosulfonated ionomers.[8,9]

A unique characteristic of BCPs is their tendency to microphase separate, a process driven by the chemical incompatibilities between the different components of the copolymer.[10] Most polymeric species are immiscible with each other, as even minor chemical differences between the distinct blocks produce enough excess enthalpy to make mixing unfavorable. In block copolymers distinct blocks segregate into well-defined mesodomains to minimize the interfacial contact between them, producing an array of nanostructures, e.g., spherical, cylindrical, and the double gyroid network morphology. In linear AB diblock compolymers, essentially two canonical parameters govern the phase BCPs phase behavior: the copolymer volumetric composition, f, and the degree of segregation, χN, where χ is the Flory–Huggins interaction parameter (thermal energy per lattice site with volume V_{ref}) and

$$N = \frac{V_{polymer}}{V_{ref}} = \frac{1}{N_{av}V_{ref}}\left(\frac{M_{n,A}}{\rho_A} + \frac{M_{n,B}}{\rho_B}\right) \quad (1)$$

is the renormalized degree of polymerization (number of lattice sites per polymer; ρ is the mass density of block I; $M_{n,i}$ is the number average molar mass of block i). χ describes the free energy cost per lattice site of contacts between A and B monomers[10] and has been tabulated for numerous binary systems.[11] χ is typically small and positive such that for typical molecular weights (i.e., 10−100 kDa) the product $\chi N \sim 10^1$−10^2, signifying a net repulsion between A and B. For example, for polystyrene/polyisoprene, χ_{SI} is of order 0.1.[12] An abundance of the available coarse-grained statistical theories describing heterogeneous polymer thermodynamics employ χ

as the thermodynamic force that drives microphase separation.[10] These theories can be further divided into three categories: (i) the strong segregation limit (SSL, $\chi N \gg 100$), (ii) the weak segregation limit (WSL, $\chi N \leq 10$), with (iii) the intermediate segregation regime spanning the two extremes.

Only sparse information has been published thus far on the χ of highly segregated polyanionic block copolymers and on the effects that the degree of sulfonation and temperature have on the χ.[3,13,14] Zhou et al. determined the concentration profiles in bilayer films of deuterated polystyrene and lightly sulfonated PS_S ($x \leq 2.6\%$, where x denotes the mole fraction of sulfonated styrene units) with forward recoil spectrometry (FRES) and interpreted the results in the context of classical Flory–Huggins theory.[14] This research concluded $26.2 \leq \chi_{S/S_S} \leq 77.7$, clearly beyond the purview of mean-field theory; moreover, in this study the S_S concentrations used for χ calculation were $0.7\% \leq x \leq 1.2\%$—far too small for the application of a mean-field description or for the approximation of a composition-independent χ.

A number of other studies have reported the phase behavior of S_S-containing di- and triblock copolymers. Poly(S_S-*block*-ethylene butylene-*block*-S_S) ($S_S E_B S_S$) has been frequently investigated as an alternative to Nafion in direct methanol fuel cells. Kim, Kim, and Jung, for example, examined the role of sulfonation extent in water and methanol transport in a 118 kDa $S_S E_B S_S$, which was found to form cylinders with a d-spacing of ≈ 36 nm.[15] These authors reported no change in d-spacing over the range of sulfonation extents ($0\% \leq x \leq 34\%$) considered, which is highly unusual, particularly in light of the magnitude of the interaction parameters involved. Won et al. investigated methanol crossover in an 80 kDa $S_S E_B S_S$, with $f S_S = 0.28\%$ and $x = 0.45$, and found with small X-ray scattering (SAXS) that $d = 43$ nm in the dry material.[16] No order-to-disorder transition (ODT) was reported. Mauritz et al. conducted similar experiments with a 70 kDa, $f = 0.3$, $x = 12\%$ $S_S E_B S_S$ and found $d = 26.2$ nm and $T_{ODT} = 285$ °C.[17]

Rubatat et al. examined the role of volume fraction and sulfonation extent in a series of poly(S_S-*b*-methyl methacrylate) diblocks and reported an evolution of the initially cylindrical morohpology to the lamellar phase, coupled with an increase in the d-spacing, as the sulfonation extent was increased.[18] Lee et al. investigated the proton conductivity of a poly(S_S-*b*-dimethylsiloxane) 179 kDa ($S_S D$) diblock copolymer ($f_{S_S} = 0.7$), finding only poorly ordered structures with and a surprisingly small d-spacing of 30.7 nm by SAXS, although AFM/SEM images showed structural features on the order of 50–100 nm.[19] Mays and co-workers have recently reported random phase-separated morphologies in the bulk, and tapered rodlike micelles in aqueous solution, from diblocks comprised of S_S and fluorinated polyisoprene.[20,21] The most comprehensive phase behavior study in S_S BCPs to date was conducted in 2008 by Park and Balsara,[3] in a series of symmetric poly(S_S-*b*-ethylenepropylene) ($S_S E_P$; E_P is also known as polymethylbutylene) polymers with varying sulfonation level x and molecular weight. These researchers found on the basis of T_{ODT} measurements and SAXS that $\chi_{S_S E_P} \approx 6.54$ and $\chi_{S_S S} \approx 5.89$ at 25 °C.

Polyolefins and their fluorinated homologues are useful constituents in S_S copolymers due to their viscoelastic properties and chemical resilience. Poly(dimethylsiloxane) is another interesting candidate due to its high surface energy, low T_g, and its ability to be selectively and quantitatively etched

from its matrix in BCPs yielding mesoporous materials.[22,23] Accordingly, block terpolymers comprised of S_S, E_P, and D offer the potential to design mechanically and chemically robust multifunctional membrane materials, e.g., targeting simultaneous proton and gas transport in fuel cell catalyst layers. Crucial to the design of such polymers is a fundamental understanding of the associated thermodynamics, in particular the binary interaction parameters. In this article we present experiments in which we determine the lamellar d-spacing and T_{ODT} of a series of symmetric diblock copolymers representing each of the three binary subsystems of S_S, E_P, and D. We then calculate χ in the context of self-consistent mean-field theory (SCMFT) at room temperature as a function of the degree of sulfonation for the strongly segregated pairs $S_S E_P$ and $S_S D$; the temperature dependence of χ_{EPD} is also calculated for weakly segregated diblocks at the ODT for which $\chi N \approx 10.5$.

■ EXPERIMENTAL SECTION

Materials. Hexamethylcyclotrisiloxane (D3, Acros) was stirred over calcium hydride and cyclohexane for 12 h prior to distillation. Isoprene (Acros) was purified by three consecutive vacuum distillations from *n*-butyllithium after stirring at 0 °C for 3–5 h in each case; in the last batch *sec*-butyllithium was injected and stirred for 30 min prior to distillation. Styrene (Fisher) was purified by vacuum distillation from dibutylmagnesium. *sec*-Butyllithium molarity was determined by using the Gilman double-titration method.[24,25] Cyclohexane (Fisher) was purified by passage through a Q5 (Engelhard) catalyst column and activated alumina column.[26] Tetrahydrofuran (THF) was purified by passage through activated alumina. All other chemicals were used as received without further purification.

Synthesis of Block Copolymers. All block copolymerizations were conducted with living sequential anionic polymerization in a 500 mL round-bottom flask equipped with an Airfree adapter, an injection port, and a magnetic stir bar dried for 8 h at 100 °C prior to use. Poly(styrene-*b*-isoprene) (SI) was prepared under argon, in cyclohexane as the solvent, and with *sec*-butyllithium as the initiator. Each block was reacted for 8 h at 40 °C and terminated using degassed methanol. Poly(styrene-*b*-dimethylsiloxane) (SD) was prepared in the same fashion as SI, adding a 25% mass solution of D3 in cyclohexane after the styrene polymerization was completed. The temperature was reduced to 25 °C, and 24 h was allowed to elapse to give time for the complete crossover to D polymerization. THF was then added to the reaction in a 50:50 (vol THF)/(vol cyclohexane) ratio, as the reaction needs a polar promoter to proceed.[27] The D3 addition was allowed to continue for 4 h (corresponding to 50% conversion) and was then terminated using trimethylchlorosilane. All diblock copolymers were nearly volumetrically symmetric. ID was synthesized analogously to SD.

Hydrogenation Procedure. Blocks are hydrogenated to provide them with a greater stability against degradation and prevent them from being sulfonated in the sulfonation of the styrene blocks. Hydrogenation of isoprene blocks was carried out using the procedure described by Phinyocheep et al.[28] The reaction takes place in a 2 L round-flask equipped with a stir bar and rubber septum. Polymer is added to a the reaction to obtain a solution with a concentration of 2% (w/v) polymer in *o*-xylene. A 4:1 molar ratio of *p*-toluenesulfonyl hydrazide to isoprene double bonds is added. The reaction is bubbled with argon for 30 min and then allowed to proceed for 8 h at 135 °C. The mixture is then washed several times with water and then passed through a column packed with activated basic alumina to remove byproducts. Excess solvent is evaporated, and the polymer is precipitated using a 3:1 ratio of methanol to isopropanol. The product (PSE_P) is then vacuum-dried for 48 h at 75 °C.

Sulfonation Procedure. BCPs were sulfonated following the procedures described by Makowski.[29] Styrenic polymers were dissolved in a 10:1 ratio of dichloroethane to polymer and stirred at 40 °C under argon. Acetyl sulfate was prepared by mixing

stoichiometric amounts of acetic anhydride and dichloroethane in a round-bottom flask and purged with argon; the solution was then cooled to 0 °C followed by the injection of sulfuric acid. Acetyl sulfate was added to the reaction flask containing the polymer. The reaction was allowed to proceed for 2 h and terminated using isopropanol. Different degrees of sulfonation were obtained by increasing the amount of acetyl sulfate added to the reaction. The product was purified, using the technique described by Park et al.:[3] 7 days of dialysis against running water in a cross-flow configuration, using a cellulose dialysis membrane with a 3.5 kg/mol molecular weight cutoff. The polymer was recovered using a rotary evaporator and vacuum-dried for at least 48 h at 75 °C. Degree of sulfonation (x, % styrene units sulfonated) was calculated using the procedure described by Park et al.[3]

The complete reaction procedure is summarized in Scheme 1.

Scheme 1. The Three Procedures Used To Synthesize the Different Diblocks: (a) Hydrogenation of the PS-b-PI Diblock, Followed by the Sulfonation of the PS-b-E_P Diblock; (b) Sulfonation of the PS-b-D Diblock; (c) Hydrogenation of the PI-b-D Diblock
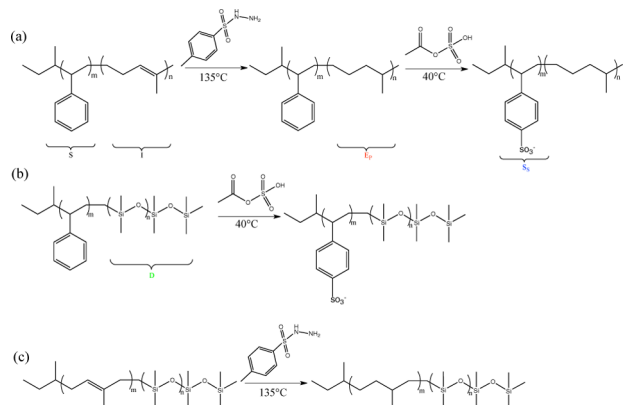
Molecular Characterization. ^{1}H NMR spectra were determined on a Varian VXR-300 spectrometer in deuterated chloroform (CDCl$_3$) or a 50/50 deuterated tetrahydrofuran/D$_2$O solution at room temperature. Molecular weights and molecular weight distributions were determined via gel permeation chromatography (GPC) with respect to polystyrene standards, using HPLC chloroform as the solvent, in a Waters 717 autosampler and a Waters 515 HPLC system using a Waters 2414 refractive index detector. A HPLC tetrahydrofuran GPC was used for samples that were not soluble in chloroform. Representative NMR spectra and GPC traces appear in the Supporting Information.

Transmission Electron Microscopy (TEM). Real-space images of BCPs were collected with a Tecnai G^2 F20 scanning/transmission electron microscope at a high tension voltage of 200 kV by either solvent casting (water/THF) the BCPs onto copper grids coated with a holey carbon film and annealed for 2 h at 80 °C or by ultrathin (≈80 nm) sectioning of the BCPs at cryogenic temperature using a Leica Ultramicrotome Ultracut 125UCT, with a Leica EM FCS cryo-stage. The water/THF concentration was varied for each sample to verify that solvent selectivity was influencing the observed phase behavior; samples were allowed to dry slowly over the course of 120 h in a controlled environment. Scanning electron microscope (SEM) experiments were conducted on a FEI Quanta-250 field emission at a voltage of 10 kV, cryo-fracturing the sample prior to imaging. D-containing samples were imaged using natural contrast. RuO$_4$ vapors were used to stain S_SE_P samples.

Small-Angle X-ray Scattering. Small-angle X-ray scattering experiments were conducted on a Rigaku copper Kα source instrument. The microfocus cathode source was operated at 40 kV and 30 mA, and the charge-coupled device (CCD) detector measured the X-ray scattering in picoamperes. Samples were enclosed in Kapton

tape and suspended in a temperate-controlled holder (maximum heating temperature 350 °C) inside an evacuated chamber with a sample-to-detector distance of 2 m. Silver behanate was used as a calibration standard. PS$_S$-b-D X-ray scattering was measured using an Anton Paar SAXSess instrument (SAXSess) instrument located at the Characterization Facility at the University of Minnesota—Twin Cities. Samples were placed in a Cu sample holder, and scattering was measured at room temperature for 25 min, operating at 40 kV and 50 mA.

Viscoelastic/Thermal Characterization. A TA Instruments ARES-LS1 strain-controlled rheometer with a convection oven was used to test the diblocks rheology under nitrogen gas flow to prevent polymer degradation. Samples were tested in a parallel plate geometry using a temperature ramp test at heating rate of 5 °C and a strain of 2%. Rheology data were not obtainable from sulfonated BCPs due to their highly brittle nature and absence of a glass transition below 200 °C.

DSC experiments were conducted on a TA Instruments Q2000 differential scanning calorimeter equipped with liquid nitrogen cooling system (LNCS). Three consecutive heating and cooling runs where done for each sample (−100 to 200 °C) using standard aluminum pans.

■ RESULTS

We have synthesized a total of 28 compositionally symmetric *AB* diblock copolymers for this study, representing each of the three binary pairs in the $S_S/E_P/D$ system and four sulfonation levels in each S_S-containing material. The *A*-block volume fraction for each specimen lies between 0.44 and 0.54, where the lamellar (LAM) phase is known to be the equilibrium phase in other diblock copolymers.[12,30] All of the samples exhibited low polydispersity (<1.05). A summary of the molecular and morphological characteristics of the S_SE_P, S_SD, and E_PD and copolymers appears in Table 1. Chain contour length $l = \sum_i^n l_i$, with n as the number of backbone bonds and l_i the bond length, was estimated using bond lengths $l_{C-C} \approx 1.54$ Å and $l_{Si-O} \approx 1.63$ Å. As discussed in further detail below, SAXS and TEM were used to characterize the morphology of each polymer and measure the d-spacing. We found that S_S-containing diblocks had no experimentally accessible order−disorder transition temperature (T_{ODT}), even at the lowest molecular mass and sulfonation extent.

Thermal Analysis. It is well established that sulfonation has a strong influence on the polystyrene glass transition temperature (T_g).[19,32] Representative DSC cooling traces for S_SE_P appear in the Supporting Information. In each specimen there is a pseudodiscontinuity in the slope of the heat flow near −55 °C, corresponding to the T_g of the E_P block. However, there is no such inflection at higher temperatures up to the maximum of 200 °C, indicating that S_S is vitreous throughout the experimentally applicable temperature range. For this reason thermal annealing of S_S diblocks was not possible, and samples for morphological characterization were dissolved in a tetrahydrofuran (THF)/H$_2$O solution and allowed to dry in a controlled environment over the period of 5 days. (THF is a nonsolvent for S_S; H$_2$O is a nonsolvent for E_P and D; mixtures of THF/H$_2$O are of the few solvents capable of solvating these polymers.) Moreover, attempts to process block copolymers into disks for rheology were unsuccessful at processing temperatures up to 200 °C; these polymers remained brittle and powder-like, further evidence of the absence of a S_S T_g in this temperature range.

Rheology. The dynamic elastic modulus $G'(\omega,T)$ of E_PD specimens was measured as a function of temperature at a scan rate of 1 (°C/min) in the parallel plate configuration of a stress-

Table 1. Molecular and Morphological Characteristics of the S_SE_P, S_SD, E_PD, and Diblock Copolymers Synthesized for This Study

sample	M_n (kDa)	N^a	PDI	f_A (vol %)	X (mol %)	l (nm)	$R_g{}^b$ (nm)	D^{*c} (nm)
S_SE_P 3KA	3.2	61	1.04	0.44	0.28	9.7	3.6	8.1
S_SE_P 3KB	3.2	61	1.04	0.44	0.33	9.7	3.6	8.4
S_SE_P 3KC	3.2	61	1.04	0.44	0.51	9.7	3.6	9.0
S_SE_P 6KA	6.2	119	1.02	0.46	0.17	18.8	4.9	6.0
S_SE_P 6KB	6.2	119	1.02	0.46	0.77	18.8	4.9	10.3
S_sEp 6KC	6.2	119	1.02	0.46	0.80	18.8	4.9	10.8
S_SE_P 6KD	6.2	119	1.02	0.46	0.92	18.8	4.9	12.1
S_SE_P 9KA	9.2	177	1.02	0.44	0.19	28.0	6.0	11.6
S_sE_p 9KB	9.2	177	1.02	0.44	0.32	28.0	6.0	11.8
S_SE_p 9KC	9.2	177	1.02	0.44	0.82	28.0	6.0	14.7
S_sE_p 12KA	12.2	234	1.02	0.46	0.21	37.0	6.8	12.6
S_sE_P 12KB	12.2	234	1.02	0.46	0.65	37.0	6.8	17.7
S_SE_P 12KC	12.2	234	1.02	0.46	0.73	37.0	6.8	18.3
S_SD 6KA	6.2	111	1.05	0.44	0.42	18.8	4.9	35.3
S_SD 6KC	6.2	111	1.05	0.44	0.53	18.8	4.9	36.7
S_SD 6KB	6.2	111	1.05	0.44	0.67	18.8	4.9	40.8
S_SD 6KD	6.2	111	1.05	0.44	0.78	18.8	4.9	43.2
S_SD10KA	10.4	185	1.03	0.48	0.15	31.5	6.2	27.6
S_SD10KB	10.4	185	1.03	0.48	0.27	31.5	6.2	49.5
S_SD10KC	10.4	185	1.03	0.48	0.61	31.5	6.2	58.0
S_SD10KD	10.4	185	1.03	0.48	0.73	31.5	6.2	59.4
S_sD 13KA	13.3	238	1.02	0.46	0.12	40.4	7.1	34.4
S_sD 13KB	13.3	238	1.02	0.46	0.15	40.4	7.1	40.8
S_sD 13KC	13.3	238	1.02	0.46	0.21	40.4	7.1	50.7
E_PD 6K	6.0	118	1.03	0.51		18.1	6.0	10.6
E_PD 9K	9.0	178	1.18	0.54		27.1	7.4	14.2
E_PD 11K	11.5	226	1.02	0.46		34.9	8.2	19.0
E_PD15K	15.2	300	1.02	0.50		46.0	9.5	25.2

^{a}According to eq 1 using $v_0 = 100$ Å and data from ref 31. ^{b}For a diblock copolymer with blocks i and j, $N_i = f_iN$, and $b_i{}^2 \equiv (6R_g{}^2/M)/(N/M)$, $R_g = (N_ib_i{}^2/6 + N_jb_j{}^2/6)^{1/2}$. $6R_g{}^2/M$ data were used as tabulated by Fetters et al. at 140 °C.[31] ^{c}At 25 °C.

controlled rheometer at a frequency of 0.5 Hz (π rad/s). $G'(T)$ data plotted over the relevant temperature ranges for E_PD 6K, 9K, and 11K appear in the Supporting Information. $G'(T)$ for each specimen exhibits a plateau modulus of ≈300 Pa until a critical temperature beyond which the modulus suddenly drops to below the measurement threshold of the instrument; this temperature is known to correspond to the T_{ODT}.[33]

Table 2. Order−Disorder Transition Temperature T_{ODT} for E_PD Diblock Copolymers As Determined from the Dynamic Elastic Modulus

sample	T_{ODT} (°C)	sample	T_{ODT} (°C)
E_PD 6K	37	E_PD 12K	>300
E_PD 9K	147	E_PD 15K	>300
E_PD 11K	245		

SAXS. Small-angle X-ray scattering was conducted to characterize the average morphology and associated d-spacing of all polymers. All specimens yielded Bragg diffraction with at least one experimentally observable primary Bragg peak; S_SE_P and E_PD patterns contained at least two visible reflections such that $q_2/q^* = 2$, where q^* and q_2 correspond to the center of the first and second peaks, consistent with the lamellar morphology; representative SAXS data for the S_SE_P series appear in the Supporting Information. The lamellar period (d-spacing) was calculated from the relationship $d = 2\pi/q^*$.

E_PD samples, summarized in Figure 1, yielded similar scattering patterns with a drop in intensity and broadening of
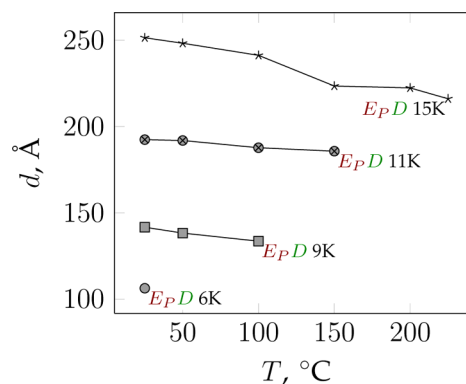
Figure 1. d vs T for E_PD as discerned from SAXS data ($d = 2\pi/q^*$).

the first-order peak at temperatures beyond the T_{ODT}, characteristic of the disordered state, in agreement with the rheological measurements. The raw 1D scattering patterns are available in the Supporting Information. SAXS patterns of S_SD samples were collected using the SAXSess instrument at Characterization Facility of the University of Minnesota. The SAXSess features a q-range that approaches the ultrasmall-angle scattering regime, allowing resolution of structural features approaching $d_{max} \approx 80$ nm ($q_{min} \approx 0.008$ Å^{-1}), although interference with the direct beam is a concern for $q < 0.015$

Å^{-1}. $S_S D$ was found to scatter only weakly; this may be explained by assuming the S_S mass density is equal to the value reported by Fetters for PS,[31] which provides an estimate of the electron density of S_S of $\rho_{e,S_S} = 0.489$ (mol e$^-$)/cm^3, while that of D is $\rho_{e,D} = 0.484$ (mol e$^-$)/cm^3. Poor scattering contrast in conjunction with Bragg peaks near the instrumental detection limit reduces the quality of the resultant scattering patterns, which appear in the Supporting Information. A blank sample was used to collect the background scattering, which was removed from the $S_S D$ patterns to provide for adequate assignment of peak positions. Only first-order peaks were resolvable, which were fit with least-squares regression to a seventh-order polynomial; the reported peak position represents the root of the derivative corresponding to the peak maximum.

TEM. S_S-containing polymers were dissolved in THF/H$_2$O mixtures ranging from 30 to 70 vol % THF, drop-cast onto copper TEM grids, and covered to control the evaporation rate such that drying occurred over a period of 5 days. The solvent concentration was varied to ensure that the resultant morphology is not due to solvent selectivity. $S_S D$ grids were imaged without further staining, as D the block has natural contrast. $S_S E_P$ specimens were stained over RuO$_4$ vapors, resulting in selective association with the domains due to the absence of reactive moieties in the E_P domains. Representative TEM images of the materials appear in Figures 2 and 3. The morphology of the TEM images was consistent with the lamellar morphology, and apparent d-spacings were in good agreement with the SAXS data.

SCMFT. SCMFT calculations were conducted to determine the precise values of χN_{ODT}^{SCMFT} for the $E_P D$ specimens used in this study, accounting for differences in statistical segment length and deviations from perfect compositional symmetry. A description of our implementation of SCFMT appears in the Supporting Information. Experimental parameters and their theoretical equivalents appear in Table 3, using a reference volume of $\nu_0 = 100$ Å^3 = 60.2 cm^3/mol. These considerations increase χN_{ODT}^{SCMFT} from the accepted value of 10.495, which is valid for systems with $a_A = a_B$ and $f = {}^1/_2$. Our results appear in Figure 4 and Table 4. Table 4 also includes the location of the ODT according to the Brazovskii−Leibler−Fredrickson−Helfand (BLFH) theory which extends Leiber's random phase approximation (RPA) to account for fluctuation effects in diblock copolymers in an approximate manner.[34,35] A main result of BLFH theory is an N-dependence on the location of phase transitions; for example, for a compositionally and conformationally symmetric diblock copolymer ($f = {}^1/_2$, $a_A = a_B$)

$$\chi N_{ODT}^{BLFH} = 10.495 + 41.022 \tilde{N}^{-1/3} \qquad (2)$$

$$\tilde{N} = \frac{6 R_g^{\,2}}{\nu_0^{\,2/3}} \qquad (3)$$

For a general diblock copolymer

$$\chi N_{ODT}^{BLFH} = \chi N_s^{RPA} + C \tilde{N}^{1/3} \qquad (4)$$

where χN_s^{RPA} is the spinodal stability limit of the disordered phase according to the RPA and the constant C is determined through the BLFH theory by calculating the point at which the free energy of the disordered state is equal to that of the most
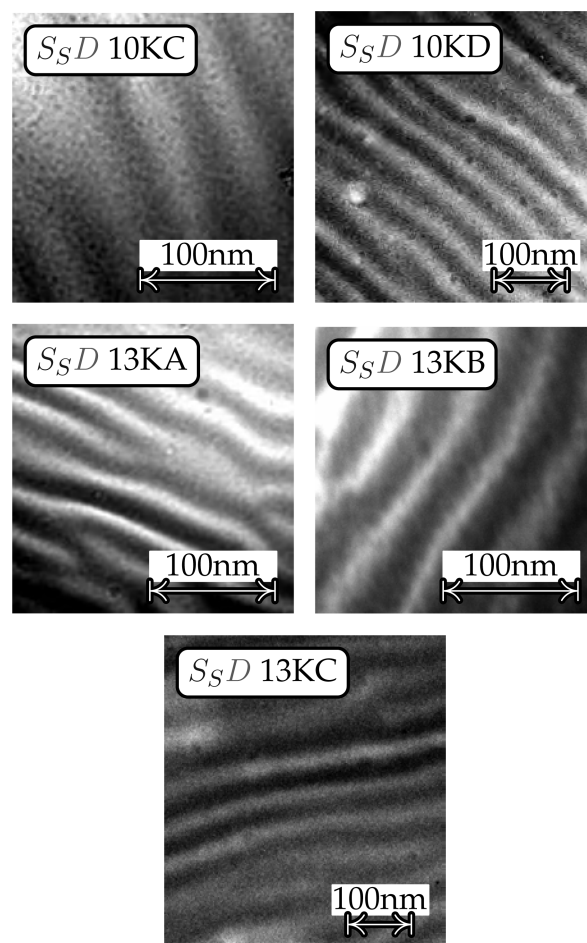

Figure 2. Representative TEM images of solvent-cast (THF + H$_2$O) $S_S D$. Dark regions are rich in D. The microscopy data are consistent with a lamellar morphology with d-spacings that are consistent with the more reliable SAXS measurements.
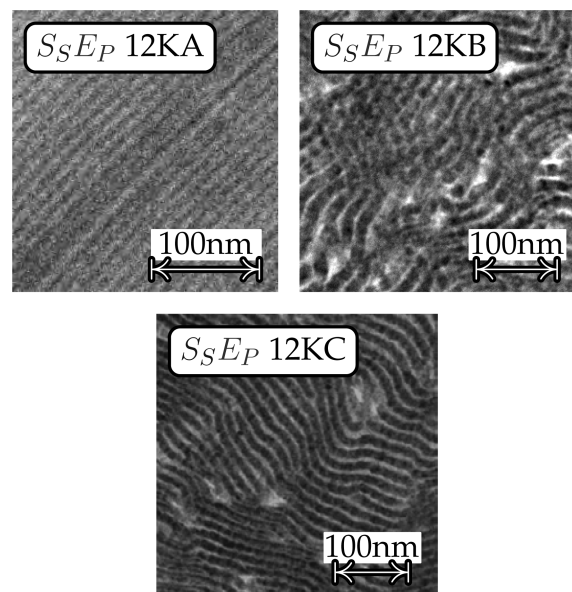

Figure 3. Representative TEM images of solvent-cast (THF + H$_2$O) $S_S E_P$ (RuO$_4$-stained). Dark regions are richer in S_S. The microscopy data are consistent with a lamellar morphology with d-spacings that are consistent with the more reliable SAXS measurements.

Table 3. Physical Property Parameters for SCFMT Calculations

species	M_0 (Da)	ρ^a (g/cm^3)	N/M (segments/ kDa)	V^b (cm^3/mol)	R_0^2/M^c (Å^2/Da)	a (Å/ segment)
S_s	184	0.969	17.1	189.9	0.245^d	3.78
E_p	70	0.790	21.0	88.6	0.645	5.54
D	74	0.895	18.6	82.7	0.457	4.96

^{a}From ref 31. ^{b}Molar volume. ^{c}Unperturbed mean-square end-to-end distance. From ref 31. ^{d}From $R_2^0/M = 0.434$ Å^2/Da for polystyrene, approximating $R_{0,S_s} \approx R_{0,PS}$.
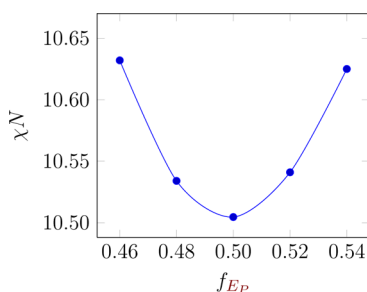
Figure 4. $\chi N_{\mathrm{ODT}}^{\mathrm{SCMFT}}$ for E_pD, as calculated using the experimental values for conformational asymmetry appearing in Table 3.

Table 4. χN_{ODT} for the E_pD Polymers Considered in This Study According to SCMFT and the Fluctuation-Corrected BLFH Theory

| sample	f_A	N^a	$\tilde{N}^b$	$\chi N_{\mathrm{ODT}}^{\mathrm{SCMFT}}$	$\chi N_{\mathrm{ODT}}^{\mathrm{BLFH}}$
E_pD 6K	0.51	118	999	10.583	14.684
E_pD 9K	0.54	178	1538	10.632	14.183
E_pD 11K	0.46	226	1850	10.625	13.965
E_pD 15K	0.50	300	2511	10.505	13.521

^{a}According to eq 1 using $v_0 = 100$ Å and data from ref 31. $^b\tilde{N} \equiv 6R_g^2/v_0^{2/3}$. This normalization was defined Fredrickson and Helfand in their development of the BLFH theory.[35]

stable ordered phase (e.g., lamallae). $\chi N_{\mathrm{ODT}}^{\mathrm{BLFH}}$ values in Table 4 were calculated in this manner.

We also determined the precise SCMFT prediction for the lamellar d-spacing as a function of χN for S_sD and S_sE_p as shown in Figure 5. These calculations provide a direct approach for estimating $\chi(T)$ through measurements of $d(T)$.

■ DISCUSSION

The data presented above contain a wealth of information regarding the thermodynamic behavior of the $S_S/E_P/D$ family
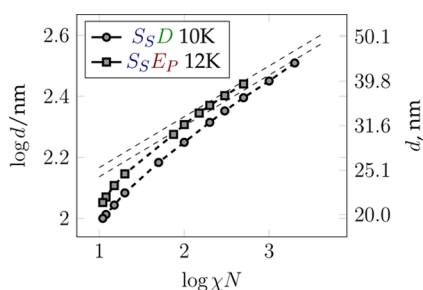
Figure 5. Lamellar d-spacing prediction from self-consistent mean-field theory for S_sD 10K and S_sE_p 12K as a function of χ. Dashed lines show Semenov's SSL prediction ($d \propto \chi^{1/6}$).[36]

of block copolymers. In this section we analyze these data within the context of Helfand's mean-field theory to deduce the relevant χ parameters. While its formulation suggests that χ should be a universal parameter, it may be extracted through a number of contexts ranging from membrane osmometry in dilute solution; static light scattering in dilute solution; binary blend phase separation studies; small angle scattering in the disordered state; and in block copolymers, from the equilibrium morphology and comparison of experimentally determined phase transitions compared to theory. Each experiment yields a χ value slightly different than another, and best practice dictates measuring χ in the manner most closely related to that in which it will be used.[11,37]

For weakly to intermediately segregated systems with experimentally accessible T_{ODT}s, the relationship $\chi(T_{\mathrm{ODT}}) = \chi_{\mathrm{ODT}}^{\mathrm{SCMFT}}/N$ generally correlates well with the form $\chi(T) = \alpha/T + \beta$, where the parameter α is directly related to the excess enthalpy of mixing and β the excess entropy.[12,37−39] This strategy for measuring $\chi(T)$ is ideally suited for use in conjunction with SCMFT for the prediction of phase behavior. Figure 6 shows $\chi(T^{-1})$ for E_pD where $\chi(T_{\mathrm{ODT}}^{-1}) = (\chi N)_{\mathrm{ODT}}^{\mathrm{SCMFT}}/$
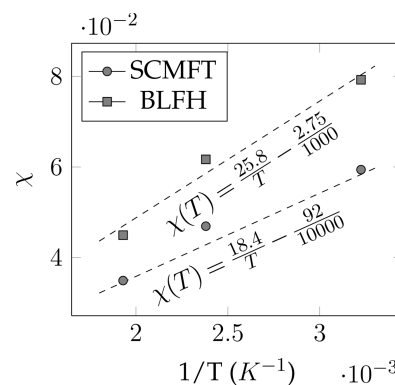
Figure 6. Correlation of $\chi(T)$ to $A/T + B$ for E_pD, where χ is determined from rheology-based T_{ODT} measurements (Table 2) and SCMFT calculations for χN_{ODT} (Figure 4). $\chi(T)$ as calculated from BLFH theory is also shown (squares) for comparison.

N, using the data from Figure 4, Table 2, and Table 4. Linear regression yields $\chi(T) = 18.4/T − 9.2/10000$. At the modest molecular weights employed in this study, fluctuation effects cause SCMFT to overestimate the stability of the disordered phase. For comparison with SCMFT, we also show the results of the BLFH treatment of fluctuation effects in Figure 6.

For intermediately segregated block polymers, the T_{ODT} can exceed the thermal decomposition temperature even at modest molecular weight and the direct measurement of $\chi(T)$ becomes more complicated. Davidock et al. made use of Semenov's SSL result[36] ($\chi N \to \infty$) that directly relates χ to d:

$$d \approx 1.1aN^{2/3}\chi^{1/6} = 2.7R_g(\chi N)^{1/6} \qquad (5)$$

in their work demonstrating the stability of the bicontinuous double gyroid phase in low molecular weight yet strongly segregated diblock copolymers.[40] d was measured directly through SAXS and then χ inferred using eq 5. Park and Balsara later included this approach in their study of S_sE_p phase behavior.[3] While this method is certainly useful for producing order-of-magnitude estimates of χ, from a quantitative perspective the sixth-order amplification of uncertainties in the measurement of d, a, and N is unfortunate. Moreover, eq 5

will only quantitatively agree with the SCFMT continuous Gaussian model in the asymptotic limit, $\chi N \gg 1000$, although the scaling relationship $d \propto \chi^{1/6}$ is approximately realized within SCMFT at much smaller values of χN, as is evident in Figure 5.

To illustrate these points, we show in Figure 7 the values of χ required within SCMFT to produce $E_P D$ lamellae with the d-
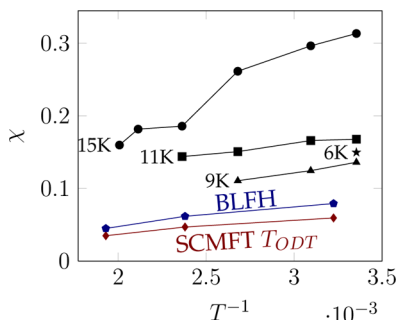

Figure 7. $\chi(T^{-1})$ for EP_D as determined from SCFMT-calculated lamellar d-spacing. The colored data are repeated from Figure 6 for comparison. While there is agreement within roughly $^{1}/_{2}$-order-of-magnitude, the strong predicted dependence of d on χ makes quantitative χ-estimates from d-spacing an unrealistic proposition, even when extra care is taken to adjust the theory (as we have) to the specific system.

spacings displayed in Figure 1. The χ-values inferred from d-spacing in Figure 7 follow the typical linear dependence in T^{-1}, yet fail to conform to a single master curve; i.e., there appears to be a molecular weight dependence that is not anticipated by the theory. This behavior is not a consequence of fluctuation effects as is evident by comparison of d-inferred χ^{SCMFT} values with those deduced from the BLFH theory. We expect that this is largely due to the experimental uncertainties in values for a_i, f, and N; another more fundamental aspect that may play a role is failure of the continuous Gaussian chain model to quantitatively account for the chain dimensions of the modest sizes presented in this study. An interesting extension of these experiments would be to determine if $\chi(T)$ as measured from d-spacing converges to a single curve as the molecular weight is increased. Thus, while $\chi(T)$ from d-spacing generates values of similar magnitude to $\chi(T)$ derived from T_{ODT}, the former method appears to systematically overestimate the magnitude of the interaction parameter.

With these caveats in place, we proceed to estimate $\chi(25\ °\text{C})$ for $S_S E_P$ and $S_S D$ as a function of sulfonation extent. Figure 8 plots $\chi S_S E_P(x)$, as determined by the SCFMT d-spacing, as a function of x for the $S_S E_P$ polymers of the present study along with lamellar specimens from the study of Park and Balsara.[3] There is a considerable degree of variability among specimen which again reflects the exacerbation of small uncertainties in the molecular characteristics of each by the strong dependence of d on χ. For each family prepared from the same parent SE_P polymer, the data appear to trend monotonically with x in each case.

There are three binary interactions present in this system: (pure) S/E_P, (pure) S/E_P, and (pure) $S/(pure) S_S; i.e., the S_S block is a random copolymer of pure styrene and sulfonated styrene segments. In polymer blends such as those considered by Zhou et al.,[14] or the disordered state in block copolymers, the χ_{S/S_S} interaction can play a significant role in the qualitative thermodynamic behavior of the system, a phenomenon known as the "copolymer effect":[14,41] A binary blend of A and B may
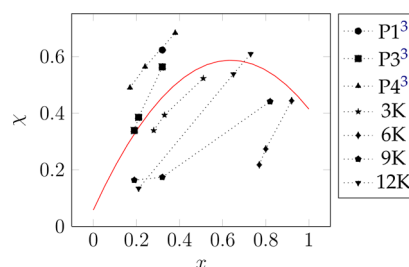

Figure 8. $\chi(25-30\ °\text{C}, x)$ for $S_S E_P$, calculated as the value required to produce the experimentally determined lamellar d-spacing in SCMFT. Calculations include the polymers of the present study (25 °C) and those from ref 3 (30 °C). Each series follows a roughly linear relationship between x and χ. The copolymer mixing theory (curve shown in red for illustrative purposes), as discussed in the text, *is not theoretically applicable to d-based interaction parameters.*

phase separate given a particular χ_{AB}. Suppose A is copolymerized with C, such that $\chi_{BC}\chi_{AC}$: a blend of A-co-C and B will have a lesser tendency to phase separate because less unfavorable B/C contacts dilute the more unfavorable A/C contacts. If A and C segments have freedom to rearrange (i.e., a statistical copolymer, or a disordered melt), the mean-field interaction energy $F^{\text{mf}} = f_A f_B \chi_{AB} + f_A f_C \chi_{AC} + f_B f_C \chi_{BC}$ factors to the familiar copolymer formula for the effective interaction parameter:[41]

$$\chi_{\text{eff}} \equiv \frac{F^{\text{mf}}}{f_{A/C} f_B} = \chi_{A/C-B} = x\chi_{BC} + (1-x)\chi_{AB}$$
$$+ x(1-x)\chi_{AC} \qquad (6)$$

where the definitions $f_{A/C} = f_A + f_C$, $f_A = (1-x)f_{A/C}$, and x as the fraction of C segments in the A/C copolymer have been invoked. The associated interaction parameters may be estimated by regression of the data in Figure 8 to the random copolymer theory, where S_S* indicates the pure S_S segment. This yields

$$\chi_{SE_P} = 0.058 \quad \chi_{S_S*E_P} = 0.415 \quad \chi_{S_S*/S} = 1.31 \qquad (7)$$

These factors indicate that because the S_S/E_P interaction is weaker than the S_S/S interaction,[3] the disordered state in S_S/E_P polymers can be promoted due to the net reduction of S/S_S contacts compared to an ordered system; this consideration is likely why some of the very low molecular weight $S_S E_P$ specimens considered by Park and Balsara were found to have accessible T_{ODT}s. *The "colpolymer" effect is relevant in the description of the ODT because the assumptions of the "copolymer effect" apply: χ_{S_S/E_P} parameters based on T_{ODT} measurements should be expected to conform to eq 6.*

On the other hand, the copolymer equation *does not* pertain to d-spacing-derived χ parameters. This is because the underlying theory is placed—by construction—into the strongly segregated state where the "dilution of contacts" argument breaks down since all A/C contacts are confined to a separate phase in which B segments are absent. Thus, the failure of eq 6 (red curve, Figure 8) to describe our data is not surprising *because it is not applicable to strongly segregated melts.*

Figure 9 shows $\chi_{S_S D}(x)$ as computed from SCFMT and the measured d-spacings in Table 1. Again, we observe different but roughly linear dependencies of the SCMFT $\chi_{S_S D}$ parameter as the sulfonation extent varies for each of the three molecular
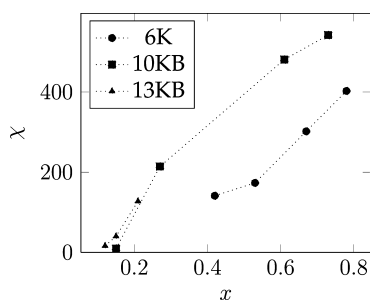
Figure 9. $\chi(25\ °C, x)$ for S_SD, calculated as the value required to produce the experimentally determined lamellar d-spacing in SCMFT. Again we observe monotonically increasing trends for all specimens; there is no evidence to support the conclusion that the copolymer mixing theory is adequate in the description of the thermodynamics of this system.

Figure 10. Ratio of the lamellar d-spacing at 25 °C to the estimated maximum d-spacing, i.e., $d/2l$.

weight series. Clearly, the nature of the S_S/D interaction is fundamentally different than that of S_S/E_P as the apparent χ is *roughly 3 orders of magnitude greater*.

In spite of the uncertainties involved with the extraction of χ from d, clearly as x tends to unity, $\chi \sim 400-600$, *according to SCMFT (and the SSL) and the continuous Gaussian chain model employed to evaluate it*. To put this value into context, according to solubility parameter theory, the S_S solubility parameter can be written as $\delta_{S_S} = d_D + (RT/V_{ref})\chi_{S_SD}^{1/2} = 204\ (\text{cal/cm}^3)^{1/2}$ at room temperature using the tabulated value[42] $\delta_D = 7.4\ (\text{cal/cm}^3)^{1/2}$ and $\chi_{S_SD} = 400$. Does this imply that SCMFT and the SSL predict that the cohesive energy density for S_S is on the order of 40 kcal/cm^3 or 575 kJ/mol (the C−C bond energy is only 348 kJ/mol)? *We think not*.

The underlying problem is that in the Gaussian chain model chains are infinitely extensible; i.e., $d \to \infty$ as $\chi \to \infty$. This is mathematically convenient, and in "traditional" polymer systems it poses no issue, since the model predicts the correct elastic restoring force to balance typical interaction strengths. However, the model is springlike to infinite extension; i.e., there is nothing in it to "tauten" the chain as it approaches its contour length. However, in a real chain the elastic potential will approach the backbone bond energy as the chain becomes fully extended, i.e., as its end-to-end distance approaches the contour length l.

Clearly then, the S_SD interaction has surpassed the limits of applicability of the Gaussian chain model, and consequently it has produced nonphysical values of χ_{S_SD}. To further illustrate this point, we summarize the d-spacing data normalized by $2l$ for all samples considered in this study as a function of x in Figure 10. The quantity $2l$ may be viewed as an upper bound for the lamellar period in a diblock copolymer system, which would be realized physically by each block stretching to its contour length. For S_SE_P and E_PD, $d/2l < 0.5$, typical of many block copolymers. In the S_SD series, however, $d/2l > 0.75$ for $x > 0.2$, approaching unity as x is increased. These observations indicate that S_SD polymers approach maximal extension given a sufficient sulfonation level.

The continuous Gaussian chain fails to describe these polymers since it includes no limit to its extensibility; that is, each differential chain segment is treated as a Hookean spring with a spring constant of $3k_BT/a^2$. Consequently, both SCMFT and SST predict $\lim_{\chi \to \infty} d = \infty$ while in the physical system $\lim_{\chi \to \infty} d = 2l$. As such, SCMFT/SST predictions in highly segregated systems such as these *cannot be relied upon* to predict
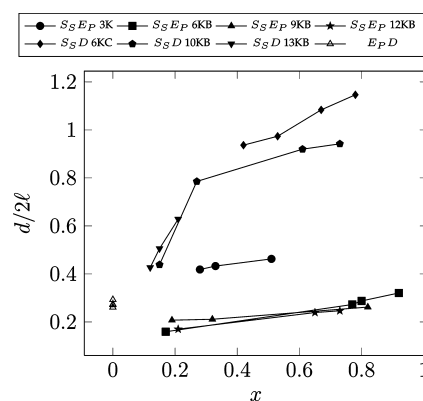
experimental behavior. This shortcoming could be alleviated by using a nonlinear chain model such the Kratky−Porod wormlike chain or a discrete bead−spring model with finite extensibility, e.g., the finitely extensible nonlinear elastic (FENE) model.[43,44] Nonetheless, once the d-spacing for a diblock copolymer system has saturated in the manner we observe for S_SD, its utility for the estimation of interaction parameters is reduced.

■ CONCLUSIONS

We have synthesized and characterized several diblock copolymers containing the three binary interactions of the ternary system S_S, E_P, and D. With the use of SAXS measurements and the use of SCFMT effective interaction parameters were calculated for the systems, yielding $\chi_{S_SD} \gg \chi_{S_SE_P} > \chi_{DE_P}$ from d-spacing measurements. We have have illustrated that the copolymer mixing equation for χ_{eff} is not appropriate for interaction parameters measured in this fashion.

Very interestingly, we have also discovered that the S_SD system is so strongly segregated that it clearly surpasses the limits of the traditional SSL and SCMFT theories commonly used to treat block copolymer systems: $\chi_{S_S/D}$ is so strong that S_SD diblock copolymers begin to extend to their contour length, placing them beyond the regime treatable with continuous Gaussian conformational statistics. This is evident from the clearly nonphysical values of χS_SD produced by the blind application of the theory to the data. Accordingly, we hope that these findings will serve as a cautionary note to future researchers wishing to use d-spacing to estimate χ.

■ ASSOCIATED CONTENT

Ⓢ Supporting Information
Our SCFMT methods and representative examples of basic characterization data. This material is available free of charge via the Internet at http://pubs.acs.org.

■ AUTHOR INFORMATION

Corresponding Author
*E-mail ecochran@iastate.edu.

Notes
The authors declare no competing financial interest.

■ REFERENCES

(1) Yarusso, D. J.; Cooper, S. L. *Macromolecules* **1983**, *16*, 1871−1880.
(2) Elabd, Y. A.; Napadensky, E.; Sloan, J. M.; Crawford, D. M.; Walker, C. W. *J. Membr. Sci.* **2003**, *217*, 227−242.
(3) Park, M. J.; Balsara, N. P. *Macromolecules* **2008**, *41*, 3678−3687.
(4) Jancar, F. K. *Polym. Eng. Sci.* **1998**, *38*, 783−792.
(5) Prater, K. B. *J. Power Sources* **1994**, *51*, 129−144.
(6) Gottesfeld, S.; Zawodzinski, T. A. *Advances in Electrochemical Science and Engineering*; Wiley-VCH Verlag GmbH: Berlin, 2008; pp 195−301.
(7) Gasteiger, H. A.; Kocha, S. S.; Sompalli, B.; Wagner, F. T. *Appl. Catal., B* **2005**, *56*, 9−35.
(8) Elabd, Y. A.; Napadensky, E. *Polymer* **2004**, *45*, 3037−3043.
(9) Weiss, R. A.; Yu, W.-C. *Macromolecules* **2007**, *40*, 3640−3643.
(10) Bates, F. S.; Fredrickson, G. H. *Phys. Today* **1999**, 32−38.
(11) Cochran, E. W.; Morse, D. C.; Bates, F. S. *Macromolecules* **2003**, *36*, 782−792.
(12) Khandpur, A. K.; Foerster, S.; Bates, F. S.; Hamley, I. W.; Ryan, A. J.; Bras, W.; Almdal, K.; Mortensen, K. *Macromolecules* **1995**, *28*, 8796−8806.
(13) Beck Tan, N. C.; Liu, X.; Briber, R. M.; Peiffer, D. G. *Polymer* **1995**, *36*, 1969−1973.
(14) Zhou, N. C.; Xu, C.; Burghardt, W. R.; Composto, R. J.; Winey, K. I. *Macromolecules* **2006**, *39*, 2373−2 379.
(15) Kim, J.; Kim, B.; Jung, B. *J. Membr. Sci.* **2002**, *207*, 129−137.
(16) Won, J.; Choi, S. W.; Kang, Y. S.; Ha, H. Y.; Oh, I.-H.; Kim, H. S.; Kim, K. T.; Jo, W. H. *J. Membr. Sci.* **2003**, *214*, 245−257.
(17) Mauritz, K. A.; Blackwell, R. I.; Beyer, F. L. *Polymer* **2004**, *45*, 3001−3016.
(18) Rubatat, L.; Li, C.; Dietsch, H.; Nykanen, A.; Ruokolainen, J.; Mezzenga, R. *Macromolecules* **2008**, *41*, 8130−8137.
(19) Lee, W.; Kim, H.; Lee, H. *J. Membr. Sci.* **2008**, *320*, 78−85.
(20) Sodeye, A. I. I.; Huang, T.; Gido, S. P.; Mays, J. W. *Polymer* **2011**, *52*, 1963−1970.
(21) Wang, X.; Hong, K.; Baskaran, D.; Goswami, M.; Sumpter, B.; Mays, J. *Soft Matter* **2011**, *7*, 7960−7964.
(22) Cavicchi, K. A.; Zalusky, A. S.; Hillmyer, M. A.; Lodge, T. P. *Macromol. Rapid Commun.* **2004**, *25*, 704−709.
(23) Todd, E. M.; Hillmyer, M. A. *Porous Polymers*; John Wiley & Sons, Inc.: New York, 2011; pp 31−78.
(24) Gilman, H.; Cartledge, F. K. *J. Organomet. Chem.* **1964**, *2*, 447−454.
(25) Ren, Y.; Lodge, T. P.; Hillmyer, M. A. *Macromolecules* **2000**, *33*, 866−876.
(26) Pangborn, A. B.; Giardello, M. A.; Grubbs, R. H.; Rosen, R. K.; Timmers, F. J. *Organometallics* **1996**, *15*, 1518−1520.
(27) Elkins, C.; Long, T. *Macromolecules* **2004**, *37*, 6657−6659.
(28) Phinyocheep, P.; Pasiri, S.; Tavichai, O. *J. Appl. Polym. Sci.* **2003**, *87*, 76.
(29) Makowski, H. S.; Lundberg, R. D.; Singhal, G. H. US Patent 4,157,432, 1977.
(30) Matsen, M. W.; Schick, M. *Phys. Rev. Lett.* **1994**, *72*, 2660−2663.
(31) Fetters, L. J.; Lohse, D. J.; Richter, D.; Witten, T. A.; Zirkel, A. *Macromolecules* **1994**, *27*, 4639−4647.
(32) Shi, Z.; Holdcroft, S. *Macromolecules* **2005**, *38*, 4193−4201.
(33) Rosedale, J. H.; Bates, F. S. *Macromolecules* **1990**, *23*, 2329−2338.
(34) Leibler, L. *Macromolecules* **1980**, *13*, 1602−1617.
(35) Fredrickson, G. H.; Helfand, E. *J. Chem. Phys.* **1987**, *87*, 697−705.
(36) Semenov, A. N. *Sov. Phys. JETP* **1985**, *61*, 733.
(37) Maurer, W. W.; Bates, F. S.; Lodge, T. P.; Almdal, K.; Mortensen, K.; Fredrickson, G. H. *J. Chem. Phys.* **1998**, *108*, 2989−3000.
(38) Han, C. D.; Kim, J.; Kim, J. K. *Macromolecules* **1989**, *22*, 383−394.
(39) Cochran, E. W.; Bates, F. S. *Macromolecules* **2002**, *35*, 7368−7374.
(40) Davidock, D. A.; Hillmyer, M. A.; Lodge, T. P. *Macromolecules* **2003**, *36*, 4682−4685.
(41) Krishnamoorti, R.; Graessley, W. W.; Balsara, N. P.; Lohse, D. J. *Macromolecules* **1994**, *27*, 3073−3081.
(42) Brandrup, J.; Immergut, E. H.; Grulke, E. A.; Abe, A.; Bloch, D. R. *Polymer Handbook*, 4th ed.; John Wiley & Sons: New York, 1999; p 2005.
(43) Kratky, O.; Porod, G. *Recl. Trav. Chim.* **1949**, *68*, 1106.
(44) Warner, H. R. *Ind. Eng. Chem. Fundam.* **1972**, *11*, 379−387.